PHYSICAL REVIEW B **96**, 041106(R) (2017)

# Evolution of the remnant Fermi-surface state in the lightly doped correlated spin-orbit insulator $Sr_{2-x}La_xIrO_4$

K. Terashima,[1,*] M. Sunagawa,[2] H. Fujiwara,[2] T. Fukura,[2] M. Fujii,[2] K. Okada,[3] K. Horigane,[1] K. Kobayashi,[1,2] R. Horie,[1] J. Akimitsu,[1] E. Golias,[4] D. Marchenko,[4] A. Varykhalov,[4] N. L. Saini,[5] T. Wakita,[1] Y. Muraoka,[1,2] and T. Yokoya[1,2]

[1]*Research Institute for Interdisciplinary Science, Okayama University, Okayama 700-8530, Japan*

[2]*Graduate School of Natural Sciences, Okayama University, Okayama 700-8530, Japan*

[3]*Aoyama Gakuin University, Sagamihara, Kanagawa 229-8558, Japan*

[4]*Helmholtz-Zentrum Berlin für Materialien und Energie, Albert-Einstein-Strasse 15, D-12489 Berlin, Germany*

[5]*Dipartimento di Fisica, Universitá di Roma "La Sapienza," P. le Aldo Moro 2, I-00185 Rome, Italy*

(Received 13 January 2017; revised manuscript received 19 June 2017; published 7 July 2017)

The electronic structure of the lightly electron-doped correlated spin-orbit insulator $Sr_2IrO_4$ has been studied by angle-resolved photoelectron spectroscopy. We have observed the coexistence of a lower Hubbard band and an in-gap band; the momentum dependence of the latter traces that of the band calculations without on-site Coulomb repulsion. The in-gap state remained anisotropically gapped in all observed momentum areas, forming a remnant Fermi-surface state, evolving towards the Fermi energy by carrier doping. These experimental results show a striking similarity with those observed in deeply underdoped cuprates, suggesting the common nature of the nodal liquid states observed in both compounds.

DOI: 10.1103/PhysRevB.96.041106

Unconventional physics of superconductivity near the metal-insulator transition in strongly correlated Mott insulators has been one of the major themes in a variety of systems, such as cuprates, iron-based compounds, heavy-electron systems, and organic materials [1]. Recently, much attention has been given to $5d$-electron systems in which the magnitude of spin-orbit coupling is comparable to the transfer-integral and Coulomb repulsion energies, and this interplay may produce possible novel phases. $Sr_2IrO_4$ is a good example of such a system for which the electronic states can be well described by considering spin-orbit coupling as well as Coulomb repulsion energy $U$ [2,3].

$Sr_2IrO_4$ is an antiferromagnetic insulator with $T_N = 240$ K, and is isostructural to one of the parent compounds of cuprate superconductors, namely, $La_2CuO_4$ [4]. Similar to the cuprates, the electronic structure is highly two dimensional, as revealed by angle-resolved photoelectron spectroscopy (ARPES) [5,6]. Unlike cuprates, to date, $Sr_2IrO_4$ has not shown superconductivity, although a possible emergence of superconductivity in this system has been theoretically predicted by carrier doping [7–10]. On the other hand, a $d$-wave gapped state and Fermi arc behavior have been observed in both the bulk [11] and surface [12–14] electronic structures of doped $Sr_2IrO_4$, similar to the cuprates. Such a similarity is puzzling and raises several questions, but this is merely due to the lack of momentum-resolved data in a wide range of doping, especially in the deeply underdoped regime. This is indeed crucial to explore if this anisotropic gap has the same origin as the pseudogap in cuprate superconductors and if the gap is related to superconductivity.

To address these unsettled issues, we have studied how this $d$-wave gapped state evolves by doping in lightly doped $Sr_{2-x}La_xIrO_4$ ($x = 0$, 0.04, 0.08) using ARPES. We have observed a dispersive in-gap state that evolves by carrier doping and coexists with the lower Hubbard band (LHB) seen in the parent compound [2]. The in-gap state appears gapped in all observed momentum ($k$) regions with anisotropy in the gap magnitude. This behavior is remarkably similar to the remnant Fermi-surface state observed in deeply underdoped cuprates [15]. The present results imply that the nodal liquid state [11] with $d$-wave gap symmetry in doped $Sr_{2-x}La_xIrO_4$ may possess a common nature with the one in cuprate superconductors.

Single crystals of $Sr_{2-x}La_xIrO_4$ ($x = 0$, 0.04, 0.08) were synthesized by the flux method [16], and were used for ARPES measurements. The La contents of the samples were determined by electron-probe microanalysis. The temperature dependence of resistivity and magnetic susceptibility of the samples are shown in the Supplemental Material [17] (Fig. S1).

ARPES experiments were performed at the 1-squared beamline of BESSY II, using a Scienta-Omicron R8000 analyzer. Circularly polarized light with $h\nu = 100$ eV was used to excite the photoelectrons. Clean surfaces for measurements were obtained by *in situ* cleaving of the samples, and they were measured in an ultrahigh vacuum of better than $1 \times 10^{-10}$ Torr. Sample surfaces did not show any sign of degradation during the measurements. The Fermi levels ($E_F$) of the samples were estimated by that of a copper plate electronically contacted with the samples. The energy and angular resolutions were set at 20 meV and 0.5° (corresponding to ~0.04 $Å^{-1}$), respectively. The data were taken at $T = 100$ K for $x = 0$ to avoid a possible charging effect [2], and $T = 40$ K for the $x = 0.04$ and 0.08 samples, except for the $T$-dependence data in Fig. 4.

Figures 1(a)–1(c) show the second derivative of ARPES intensity as a function of wave vector and binding energy for $Sr_{2-x}La_xIrO_4$ ($x = 0$, 0.04, and 0.08). The color bar is shown to represent the intensity scale. The data were taken along the high symmetry line (blue line) shown in Fig. 1(d), where the solid (dashed) lines denote the Brillouin zone with (without) the rotation of $IrO_6$ octahedra. Energy distribution curves (EDCs) at representative momenta are shown in Fig. 1(e). We have observed a number of dispersive bands up to a binding

*k-terashima@cc.okayama-u.ac.jp

 

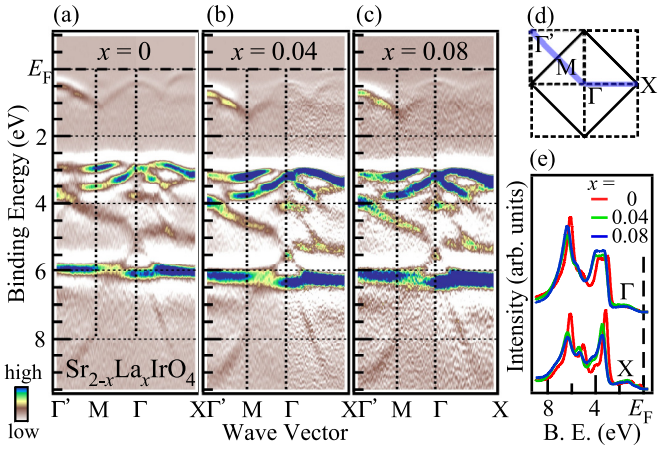


FIG. 1. (a)–(c) Second derivative of ARPES intensity plots as a function of binding energy and wave vector on $Sr_{2-x}La_xIrO_4$ ($x = 0$, 0.04, and 0.08) measured along the $k$ direction, shown as a blue line in (d). (d) The solid (dashed) line shows the folded (unfolded) Brillouin zone. (e) EDCs at the Γ and the $X$ points for $x = 0$, 0.04, and 0.08.

energy of ∼9 eV in the $x = 0$ sample. Almost identical bands are seen in the $x = 0.04$ sample, but their energy positions are shifted downward by ∼0.3 eV at every measured momentum, showing a rigid-shift-like behavior. On the other hand, the energy bands in the $x = 0.08$ sample are very close to those of the $x = 0.04$ sample, indicating that doped carriers for $x < 0.04$ shift the chemical potential and then the chemical potential is pinned against further doping up to $x = 0.08$. Such a behavior in the valence band region is consistent with an earlier observation in the near-$E_F$ region [18].

Figures 2(a)–2(c) depict the near-$E_F$ region of the band dispersions for $x = 0$, 0.04, and 0.08. See also Fig. S2 where the raw spectral intensity and EDCs are displayed for each momentum cut [17]. The overlapping gray curves are bands [11] calculated by the tight-binding method, in which both the spin-orbit coupling and on-site Coulomb repulsion ($U = 2$ eV) were taken into account. The overall character of the near-$E_F$ band dispersion in the $x = 0$ sample has been well described by first principles calculations considering both spin-orbit coupling and $U$ and ascribed as the $J_{eff} = 3/2$ band and LHB of the $J_{eff} = 1/2$ band [2,5,6,11,18,19]. In the $x = 0.04$ and 0.08 samples, the corresponding bands (guided by gray curves) are shifted downward by ∼0.3 eV, as in the valence band region. In addition to this rigid-band behavior, we have found that additional dispersive states evolve in the vicinity of $E_F$ by electron doping—for example, a downward dispersion topped at the Γ point in ∼0.5 eV and a flatband in the $MX$ direction at ∼0.1 eV that moves downward in the $X\Gamma$ direction (shown as green dashed curves; see also Figs. S2 and S3 [17]). With increasing carrier number, these bands become more clear while the LHB becomes smeared out. This tendency is also visible in EDCs of the $x = 0.04$ and 0.08 samples at the $X$ point shown in Fig. 2(d), where the spectral intensity of LHB at ∼0.5 eV (gray bar) decreases while that of the in-gap state at a lower binding energy (purple bar) increases by electron doping (see also Fig. S2 [17]). The inset of Fig. 2(d) shows the intensity ratio between LHB and the near-$E_F$ structure shown by the bars in Fig. 2(d).

The present data show that two types of dispersive states coexist in the lightly doped region and doped carriers seem responsible for moving the spectral weight from LHB at a high binding energy to an in-gap state at a low binding energy. It should be mentioned that the concept of weight transfer has been already used in an earlier ARPES study of EDCs at high symmetry points [18]. Here, we show it explicitly by revealing that both states exist as dispersive bands. Such a coexistence of two states has not been observed in an earlier ARPES study on the $x = 0.1$ sample [11]. Thus it is inferred that the spectral weight in LHB might have disappeared with a small additional electron doping upon the present $x = 0.08$ sample.

To obtain further insight into the in-gap states, we have investigated the $k$ dependence in detail. Figures 3(a)–3(c) show ARPES intensity plots as a function of two-dimensional wave vectors in $Sr_{2-x}La_xIrO_4$ at different binding energies that depict the energy contour at the top of the occupied state for each sample. As in Fig. 3(a), the top of the LHB in the parent compound appears at the $X$ point, while the momentum distribution of the in-gap state in the $x = 0.04$ and 0.08 samples resembles that in the nodal liquid state reported in a sample with a higher electron doping ($x = 0.10$) [11]. In Figs. 3(d) and 3(e), we have plotted EDCs extracted for various $k$ points along this energy contour. The corresponding positions of the $k$ points are defined by the directional angle ($\theta$)

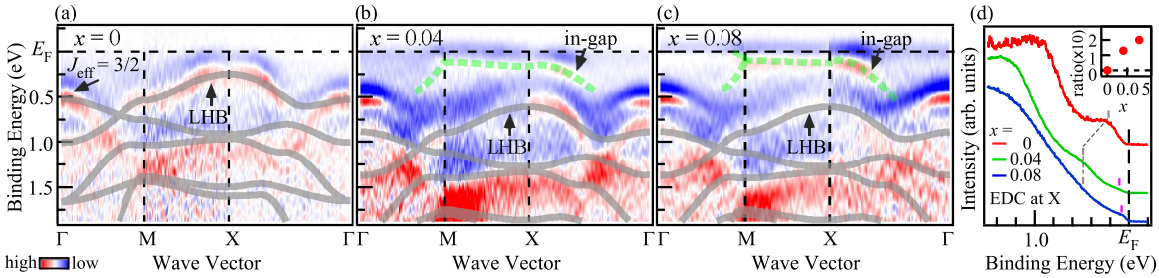


FIG. 2. (a)–(c) Second derivative of ARPES intensity plots in the near-$E_F$ region along the high symmetry line on $x = 0$, 0.04, and 0.08, respectively. Overlaid gray curves in (a) are bands calculated by the tight-binding method [11] where the on-site Coulomb repulsion energy is 2 eV. The same curves are shown in (b) and (c) after shifting downward by 0.3 eV, according to the estimated energy shift of the entire valence band in Fig. 1. The green dashed curves in (b) and (c) are guides for the in-gap state (see also Figs. S2 and S3). (d) EDCs at the $X$ point for different samples. Gray bars denote the position of LHB, and purple bars denote the position of the in-gap state. The inset shows the relative intensity ratio at the peak/hump positions ∼0.5 and 0.1 eV as a function of doping, which depicts the relative weight of LHB and the in-gap state. The positions were chosen according to the peak positions in the second derivative of EDCs.

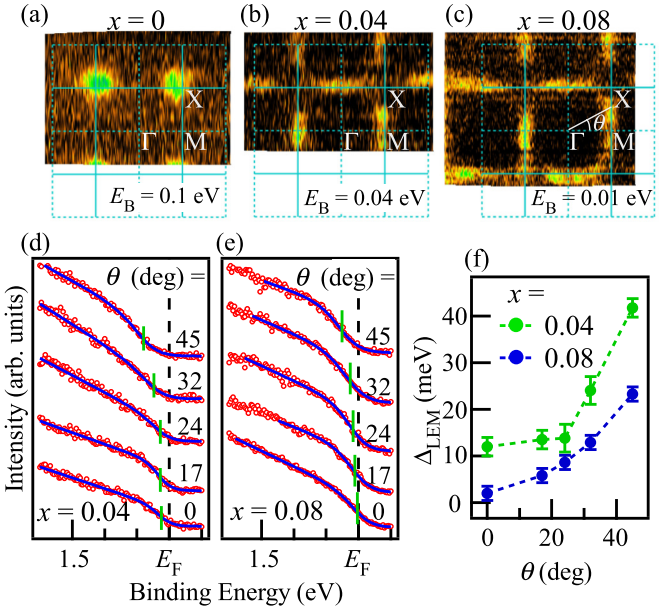


FIG. 3. (a)–(c) ARPES intensity plot as a function of two-dimensional wave vectors for $Sr_{2-x}La_xIrO_4$, $x = 0$, 0.04, 0.08, respectively. The plots were taken at the binding energies shown in each figure, with an energy-integration window of ±0.02 eV. (d) and (e) EDCs taken at various $k$ points along the energy contour on directional angles ($\theta$) for $x = 0.04$ and 0.08, respectively. Blue curves are fitting results using the Fermi-Dirac function, and green bars show the obtained positions of the leading-edge midpoint. (f) Estimated amount of energy shift in the leading-edge midpoint with respect to $E_F$ ($\Delta_{LEM}$) as a function of directional angle ($\theta$) for $x = 0.04$ (green) and 0.08 (blue).

in Fig. 3(c). The blue curves in the figures are the fitted results using the Fermi-Dirac function where we set the chemical potential term as a free parameter [20]. The leading-edge midpoint positions obtained by the fit are shown as green bars in the figure. The magnitude of the shift of the leading-edge midpoint with respect to $E_F$ has been often used to evaluate the magnitude of the gap [20,21]. It is clear from the figures that the in-gap states are gapped and the magnitude of the gap is anisotropic. In Fig. 3(f), we have shown the energy gaps estimated by the leading-edge midpoint as a function of the directional angle ($\theta$) which corresponds to the $k_F$ positions. In both constituents, the gap values tend to be the smallest along the $\Gamma M$ direction ($\theta = 0°$) and the largest along the $\Gamma X$ direction ($\theta = 45°$). With increasing doped electrons, the gapped state approaches $E_F$ while keeping its overall anisotropy in the lightly doped regime of $Sr_{2-x}La_xIrO_4$.

We show in Fig. 4 the temperature dependence of the in-gap state in $Sr_{2-x}La_xIrO_4$ ($x = 0.08$) along the $\Gamma X$ direction, taken at $T = 55$, 100, and 150 K. In order to obtain an above-$E_F$ region, the spectra were divided by the Fermi-Dirac function convoluted by the experimental energy resolution. Figures 4(d)–4(f) are curvature plots [22] derived from Figs. 4(a)–4(c). We found that while the band is modified from that of the local density approximation by the presence of a gap at low temperatures [see also Fig. S5(c) [17]], the spectral weights of the nongapped band start to be filled with a rise in temperature. As a result of such filling behavior, the

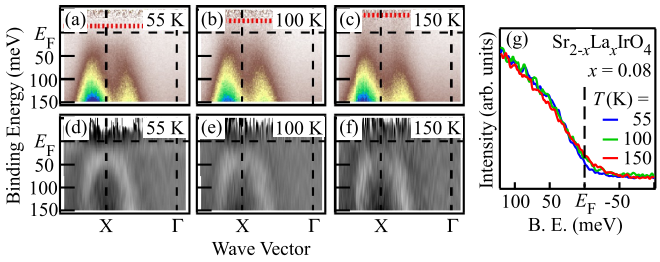


FIG. 4. (a)–(c) Temperature dependence of ARPES spectra of the $x = 0.08$ sample along the $\Gamma X$ direction divided by the Fermi-Dirac function convoluted by experimental energy resolution, and their curvature plots [(d)–(f)]. The red dashed lines in the figures denote the energy corresponding to $3k_BT$ above $E_F$. (g) EDCs of (a)–(c) at estimated $k_F$.

leading edge of the $k_F$ spectrum in Fig. 4(g) moves toward $E_F$ as the temperature rises, but it is still far from $E_F$ at $T = 150$ K, indicating that the gap has not yet completely closed at this temperature. We note that such a filling can correspond to the behavior of a pseudogap in cuprates [23].

Figure 5 illustrates the schematic electronic structure deduced from the above results. As we dope the electrons, the entire valence band including LHB shifts toward a higher binding energy and is pinned with the formation of an in-gap state. Regarding the position of the chemical potential with respect to the Mott gap, the position of LHB in doped samples (∼0.5 eV) is close to the magnitude of the Mott gap (0.54 eV) of the parent compound observed by optical spectroscopy [24]. Thus the chemical potential is expected to lie near the bottom of the upper Hubbard band (UHB), as has been proposed earlier [18], which would correspond to the case of (electron-) doped cuprates [25]. Additional carriers are consumed to move the spectral weight of the LHB band to the in-gap state below the Fermi level. Here, we stress that this in-gap state is different from UHB, judging from the shape of the band dispersion. The in-gap state forms a dispersive band with momentum dependence that tracks the calculated tight-binding band but with an anisotropic energy gap, resulting in a remnant Fermi surface (for a further comparison of $E$-$k$ dispersion with the calculation, see Fig. S5 [17]). The anisotropically gapped state approaches $E_F$ by additional carrier doping, as we observed at the $x = 0.08$ sample.

The observed remnant Fermi-surface state shows a momentum dependence and gap anisotropy similar to the nodal liquid

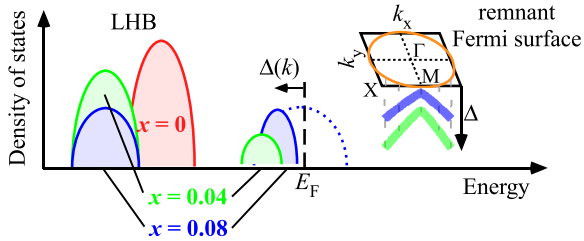


FIG. 5. Schematic graph of the doping-induced change in the electronic structure of $Sr_{2-x}La_xIrO_4$ derived from the current study. The dashed blue curve represents the tight-binding band expected to appear as an in-gap state if there is no excitation gap. The inset shows the remnant Fermi surface with gap anisotropy in the Brillouin zone.

state reported in samples with higher electron doping [11,13]. Therefore, the nodal liquid state seems to evolve from the remnant Fermi-surface state in electron-doped $Sr_2IrO_4$. Our observation of the coexistence of LHB and the remnant Fermi-surface state might correspond to scanning tunneling microscopy results on $Sr_{2-x}La_xIrO_4$ where a static phase separation between the large gap state and the small gap state has been observed [26,27], while the present result is hardly reconciled with a simple phase separation of the parent material and the metallic state with a fixed doping level since the spectral line shape and gap size change with La doping, as shown in Fig. 3 [28]. Our observation of a momentum-dependent band indicates that the in-gap state would not be a completely localized state, therefore the phase separation would be, if it exists, dynamical or static with a coherence of finite distance.

Next, we compare our results of an electron-doped system with ARPES results on $Sr_2Rh_{1-x}Ir_xO_4$ [20], where the holes are effectively doped. In the hole-doped system, it has been reported that LHB approaches $E_F$ while keeping its band dispersion by hole doping. This is contrary to the electron-doped system, where we observed the emergence of an in-gap state whose momentum distribution is different from UHB. This electron-hole asymmetry in the emergence of an in-gap state upon carrier doping has been reproduced by a first principles study [29], except for the existence of an anisotropic gap [30] and a remnant Fermi surface. In the lightly hole-doped sample of $Sr_2Ir_{1-x}Rh_xO_4$, $x = 0.04$, LHB lies just below $E_F$ with energy gaps in the entire $k$ region and with an anisotropy similar to a higher hole doping. In this context, the remnant Fermi surface seems to commonly exist in hole-doped and electron-doped systems, although the gap anisotropy is reported to be Fermi-surface dependent in the hole-doped system while it is rather momentum dependent in the electron-doped system. Theoretical studies of such behavior on gaps with electron-hole asymmetry might play a key role in clarifying the nature of the energy gaps observed in carrier-doped strontium iridate.

Finally, we discuss the correspondence/difference between $Sr_{2-x}La_xIrO_4$ and cuprates in the lightly doped region. First, we note the correspondence in the existence of an in-gap state. The coexistence of LHB and an in-gap state has been observed in hole-doped $La_{2-x}Sr_xCuO_4$ [31] and electron-doped $Nd_{2-x}Ce_xCuO_4$ [32,33] but not in other systems such as $Ca_{1-x}Na_xCuO_2Cl_2$ [15] and $Bi_2Sr_2CuO_{6+\delta}$ [34]. The remnant Fermi-surface state has been observed in $CaCuO_2Cl_2$ where the band dispersion of the parent compound itself shows a $d$-wave gap anisotropy [15]. In the case of $Sr_{2-x}La_xIrO_4$, the parent compound does not show such a $d$-wave gap anisotropy and the dispersion is well described by a band calculation with a spin-orbit interaction and $U$ [2], while the in-gap state shows the behavior of a remnant Fermi surface. Second, we mention the correspondence in the gap anisotropy as a function of doping. Despite these differences, the remnant Fermi-surface state shows a common feature as in cuprates in that the gapped states approach $E_F$ by carrier doping and keep their overall gap anisotropy [34]. The present observation of a remnant Fermi-surface state suggests that the $Sr_{2-x}La_xIrO_4$ system approaches a metallic state by carrier doping in a highly corresponding manner with cuprate superconductors.

In summary, we have studied the electronic structure of lightly electron-doped $Sr_{2-x}La_xIrO_4$. We have found that a remnant Fermi surface is formed with an anisotropic gap, which approaches $E_F$ and acquires a spectral weight with increasing doped carriers. These features show a close similarity to those in cuprate superconductors, implying a common nature for nodal liquid states observed in both systems.

K.T. would like to thank Dr. K. Siemensmeyer for the Laue apparatus. The authors are grateful to K. Tomimoto at the Center for Instrumental Analysis for the measurements of the elemental analyses. K.T. and T.W. would like to acknowledge the hospitality at the Sapienza University of Rome. The experiments have been performed at the 1-squared beamline of BESSYII. This research was partially supported by the Program for Promoting the Enhancement of Research University from MEXT, the Program for Advancing Strategic International Networks to Accelerate the Circulation of Talented Researchers from JSPS (R2705), and JSPS KAKENHI (Grants No. 25000003 and No. 15H05886). This work is a part of the executive protocol of the general agreement for cooperation between the Sapienza University of Rome and Okayama University, Japan.

[1] D. J. Scalapino, Rev. Mod. Phys. **84**, 1383 (2012).
[2] B. J. Kim, H. Jin, S. J. Moon, J.-Y. Kim, B.-G. Park, C. S. Leem, J. Yu, T. W. Noh, C. Kim, S.-J. Oh, J.-H. Park, V. Durairaj, G. Cao, and E. Rotenberg, Phys. Rev. Lett. **101**, 076402 (2008).
[3] B. J. Kim, H. Ohsumi, T. Komesu, S. Sakai, T. Morita, H. Takagi, and T. Arima, Science **323**, 1329 (2009).
[4] M. K. Crawford, M. A. Subramanian, R. L. Harlow, J. A. Fernandez-Baca, Z. R. Wang, and D. C. Johnston, Phys. Rev. B **49**, 9198 (1994).
[5] Q. Wang, Y. Cao, J. A. Waugh, S. R. Park, T. F. Qi, O. B. Korneta, G. Cao, and D. S. Dessau, Phys. Rev. B **87**, 245109 (2013).
[6] A. Yamasaki, H. Fujiwara, S. Tachibana, D. Iwasaki, Y. Higashino, C. Yoshimi, K. Nakagawa, Y. Nakatani, K. Yamagami, H. Aratani, O. Kirilmaz, M. Sing, R. Claessen, H. Watanabe, T. Shirakawa, S. Yunoki, A. Naitoh, K. Takase, J. Matsuno, H. Takagi, A. Sekiyama, and Y. Saitoh, Phys. Rev. B **94**, 115103 (2016).
[7] F. Wang and T. Senthil, Phys. Rev. Lett. **106**, 136402 (2011).
[8] H. Watanabe, T. Shirakawa, and S. Yunoki, Phys. Rev. Lett. **110**, 027002 (2013).
[9] Y. Yang, W.-S. Wang, J.-G. Liu, H. Chen, J.-H. Dai, and Q.-H. Wang, Phys. Rev. B **89**, 094518 (2014).
[10] Z. Y. Meng, Y. B. Kim, and H.-Y. Kee, Phys. Rev. Lett. **113**, 177003 (2014).
[11] A. de la Torre, S. McKeown Walker, F. Y. Bruno, S. Riccó, Z. Wang, I. Gutierrez Lezama, G. Scheerer, G. Giriat, D. Jaccard,

C. Berthod, T. K. Kim, M. Hoesch, E. C. Hunter, R. S. Perry, A. Tamai, and F. Baumberger, Phys. Rev. Lett. **115**, 176402 (2015).

[12] Y. K. Kim, O. Krupin, J. D. Denlinger, A. Bostwick, E. Rotemberg, Q. Zhao, J. F. Mitchell, J. W. Allen, and B. J. Kim, Science **345**, 187 (2014).

[13] Y. K. Kim, N. H. Sung, J. D. Denlinger, and B. J.Kim, Nat. Phys. **12**, 37 (2016).

[14] Y. J. Yan, M. Q. Ren, H. C. Xu, B. P. Xie, R. Tao, H. Y. Choi, N. Lee, Y. J. Choi, T. Zhang, and D. L. Feng, Phys. Rev. X **5**, 041018 (2015).

[15] F. Ronning, C. Kim, D. L. Feng, D. S. Marshall. A. G. Loeser, L. L. Miller, J. N. Eckstein, I. Bozovic, and Z.-X. Shen, Science **282**, 2067 (1998).

[16] N. H. Sung, H. Gretarsson, D. Proepper, J. Porras, M. L. Tacon, A. V. Boris, B. Keimer, and B. J. Kim, Philos. Mag. **96**, 413 (2016).

[17] See Supplemental Material at http://link.aps.org/supplemental/10.1103/PhysRevB.96.041106 for information on the sample characterization, ARPES data for each momentum cut, near-$E_F$ data, curvature plot of Fig. 2, and a comparison of the experimental data with a tight-binding calculation ($U = 0$).

[18] V. Brouet, J. Mansart, L. Perfetti, C. Piovera, I. Vobornik, P. LeFèvre, F. Bertran, S. C. Riggs, M. C. Shapiro, P. Giraldo-Gallo, and I. R. Fisher, Phys. Rev. B **92**, 081117(R) (2015).

[19] S. Moser, L. Moreschini, A. Ebrahimi, B. D. Piazza, M. Isobe, H. Okabe, J. Akimitsu, V. V. Mazurenko, K. S. Kim, A. Bostwick, E. Rotenberg, J. Chang, H. M. Rønnow, and M. Grioni, New J. Phys. **16**, 013008 (2014).

[20] Y. Cao, Q. Wang, J. A. Waugh, T. J. Reber, H. Li, X. Zhou, S. Parham, S.-R. Park, N. C. Plumb, E. Rotenberg, A. Bostwick, J. D. Denlinger, T. Qi, M. A. Hermele, G. Cao, and D. S. Dessau, Nat. Commun. **7**, 11367 (2016).

[21] D. L. Feng, A. Damascelli, K. M. Shen, N. Motoyama, D. H. Lu, H. Eisaki, K. Shimizu, J.-i. Shimoyama, K. Kishio, N. Kaneko, M. Greven, G. D. Gu, X. J. Zhou, C. Kim, F. Ronning, N. P. Armitage, and Z.-X. Shen, Phys. Rev. Lett. **88**, 107001 (2002).

[22] P. Zhang, P. Richard, T. Qian, Y.-M. Xu, X. Dai, and H. Ding, Rev. Sci. Instrum. **82**, 043712 (2011).

[23] T. J. Reber, N. C. Plumb, Z. Sun, Y. Cao, Q. Wang, K. McElroy, H. Iwasawa, M. Arita, J. S. Wen, Z. J. Xu, G. Gu, Y. Yoshida, H. Eisaki, Y. Aiura, and D. S. Dessau, Nat. Phys. **8**, 606 (2012).

[24] S. J. Moon, H. Jin, W. S. Choi, J. S. Lee, S. S. A. Seo, J. Yu, G. Cao, T. W. Noh, and Y. S. Lee, Phys. Rev. B **80**, 195110 (2009).

[25] P. G. Steeneken, L. H. Tjeng, G. A. Sawatzky, A. Tanaka, O. Tjernberg, G. Ghiringhelli, N. B. Brookes, A. A. Nugroho, and A. A. Menovsky, Phys. Rev. Lett. **90**, 247005 (2003).

[26] X. Chen, T. Hogan, D. Walkup, W. Zhou, M. Pokharel, M. Yao, W. Tian, T. Z. Ward, Y. Zhao, D. Parshall, C. Opeil, J. W. Lynn, V. Madhavan, and S. D. Wilson, Phys. Rev. B **92**, 075125 (2015).

[27] I. Battisti, K. M. Bastiaans, V. Fedoseev, A. de la Torre, N. Iliopoulos, A. Tamai, E. C. Hunter, R. S. Perry, J. Zaanen, F. Baumberger, and M. P. Allan, Nat. Phys. **13**, 21 (2017).

[28] The simple phase separation is unlikely based also on the macroscopic property in Fig. S1. The magnetic susceptibility of the La-doped samples with different doping levels shows the behavior of the magnetic order at different temperatures.

[29] P. Liu, M. Reticcioli, B. Kim, A. Continenza, G. Kresse, D. D. Sarma, X.-Q. Chen, and C. Franchini, Phys. Rev. B **94**, 195145 (2016).

[30] H. Wang, S.-L. Yu, and J.-X. Li, Phys. Rev. B **91**, 165138 (2015).

[31] A. Ino, C. Kim, M. Nakamura, T. Yoshida, T. Mizokawa, Z.-X. Shen, A. Fujimori, T. Kakeshita, H. Eisaki, and S. Uchida, Phys. Rev. B **62**, 4137 (2000).

[32] N. P. Armitage, F. Ronning, D. H. Lu, C. Kim, A. Damascelli, K. M. Shen, D. L. Feng, H. Eisaki, Z.-X. Shen, P. K. Mang, N. Kaneko, M. Greven, Y. Onose, Y. Taguchi, and Y. Tokura, Phys. Rev. Lett. **88**, 257001 (2002).

[33] The properties of electron-doped cuprates have been reinvestigated recently by the protected-annealing method [M. Horio *et al.*, Nat. Commun. **7**, 10567 (2016)]. Thus the coexisting behavior of LHB and the in-gap state may need to be examined if it is generic.

[34] Y. Peng, J. Meng, D. Mou, J. He, L. Zhao, Y. Wu, G. Liu, X. Dong, S. He, J. Zhang, X. Wang, Q. Peng, Z. Wang, S. Zhang, F. Yang, C. Chen, Z. Xu, T. K. Lee, and X. J. Zhou, Nat. Commun. **4**, 2459 (2013).